The land surface water and energy budgets over the Tibetan Plateau

-A quantitative investigation based on the GLDAS

Li Xu[1,2] Hui Gao[3] and Yueqing Li [2]

George Mason University, Dept. of Climate Dynamics, 4400 University Drive, Fairfax, VA 22030

Institute of Plateau Meteorology, China Meteorological Administration, Chengdu, 610072

National Climate Center, China Meteorological Administration, Beijing, 100081

Abstract

Tibetan Plateau plays an important role in the Asian Monsoon and global general circulation system. Due to the lack of quantitative observations and complicate cold season processes in high elevation terrain, however, the land surface water and energy budgets are still unexplored over this special region. In this study, the water and energy balances are detail analyzed based on recent released land surface "reanalysis" data produced by NASA Global Land Data Assimilation System by three different land models, which first ingest all available ground and satellite data into the data assimilation system over the Tibetan Plateau. The major land surface energy and water components in the annual variability are compared. The model and data assimilation skills and deficiencies are also discussed. The total heat fluxes transition from heat source to heat

sink is observed at west edge of the TP during winter. But, the area and intensive is far less than the previous hypothesized. The Budyko curve for hydrology indicates the TP is a typical dry and arid climate where the evaporation is mainly controlled by the precipitation.

1. Introduction

The Tibetan Plateau (TP), located at the southwest part of China with an average elevation higher than 4000 meters above sea level, is often called “the roof of the world.” Within this most prominent and complicated terrain of the world, the land surface processes over TP plays a very important role in general atmospheric circulation, water resource management and global climate system (Yasunari, 2007).

In general, the TP is a vital water source for East Asia. The largest rivers of East Asia, such as the Yangtze River, Yellow River and Yalong Zangbo River, etc., have their headwaters there. A large amount of water is stored in this highest and largest plateau, in the forms of glaciers, snow-packs, lakes, and rivers. The Tibetan Plateau serves as "the world water tower". It is critical to understand where these waters come from and whether the supply to these water resources has been experiencing any changes during recent global warming. In addition, land-atmosphere interaction over TP provides a profound impact on the monsoon system. Previous studies have shown that winter snow cover over the TP has a strong link with monsoon systems during spring and

summer(Hahn and Shukla, 1976; Wu and Qian, 2003), even further impacting the typhoon genesis over the west Pacific(Xie et al., 2005) .

The lack of quantitative observations of the land surface processes over TP makes it difficult to understand the energy and water cycles over this special region. There are only 115 ground weather stations over Tibetan region in the meteorological observational network managed by China Meteorological Administration. Unfortunately, these stations focus on the meteorological variables and lack observation in the land states, such as soil moisture, evapotranspiration, snow water equivalent, sensible and latent heat fluxes. There are very few field studies in the land-atmosphere interaction over the Tibetan Plateau in recent years (Xu et al., 2008). However, these field experiments have been limited in few locations and short observational periods. Most of these studies cannot give a whole accurate image about water and energy cycles over the TP because of limited observations for key land state variables. As far as the authors know, there are no complete and detailed studies on the energy and water budget over the whole Tibetan region until now.

With the advancement in the remote sensing, land surface modeling and data assimilation techniques in the recent years, NASA Global Land Data Assimilation System (GLDAS) (Rodell et al., 2004) provides a potential to study this special region where there are no traditional observations available. The goal of the GLDAS is to generate optimal fields of land surface states and fluxes by using advanced land surface model and data assimilation techniques with available satellite and ground based observational data. The GLADS reanalyzed key land surface states and fluxes by

64 different land surface models by constraining with all available observational data from
65 1979 to present, especially the satellite retrievals from NASA.

66 Comparing to offline simulations, such as Global Soil Wetness Project (GSWP-2)
67 data set, the GLDAS applied two constraints to optimal merge model and observation
68 data to obtain the best estimation. First, by forcing the land surface models with
69 observation based meteorological fields, bias on the atmospheric model-based forcing
70 can be avoided. Second, by employing data assimilation techniques, observations of land
71 surface states can be used to curb unrealistic model state. It has a longer period than the
72 GSWP-2 data set, which only covers 1986–1995 (Dirmeyer et al., 2006).

73 This paper attempts to unveil the characteristics of surface water and energy
74 budgets over the Tibetan Plateau using newly produced GLDAS reanalysis data to
75 evaluate the ability of land surface models to characterize the water and energy budgets
76 over this special region and hence to gain insight into its thermal forcing to the general
77 circulation and Asian Monsoon.

78

79 2. GLDAS reanalysis

80 In this study, authors use 1x1 degree, 3-hourly output from a 1979-present run of
81 the Mosaic (Koster and Suarez, 1996), Noah (Chen et al., 1996; Ek et al., 2003a) and the
82 Community Land Model (Dai et al., 2003) driven by GLDAS. The cold season processes
83 are critical for the modeling of land surface water and energy balance over the TP where
84 exist the largest snow-covered and glacier region outside of the Polar Regions. The detail
85 cold season processes in the Mosaic, Noah and CLM model are brief described as below:

2.1 Mosaic model

Mosaic is a biophysically based land surface model developed for providing energy and water budget to general circulation and regional models at NASA. The model was originally derived from the SiB model (Sellers et al., 1996). The model's main innovation is its attempt to account for sub-grid variability in surface characteristics through the "mosaic" approach. A grid square area containing several different vegetation regimes is divided into relatively homogeneous sub-regions ("tiles" of the mosaic), each containing a single vegetation or bare soil type. Observed vegetation distributions are used to determine the partitioning. In this version of Mosaic model, a complete snow budget is included. Snow is accumulated on the ground and canopy when the surface air temperature is below freezing. Snow albedo is controlled by the spectral and angular distribution of solar radiation incident on the surface, surface type and snow cover. Snow starts to melt on the ground or canopy if ground/canopy temperature is above or below freezing point respectively.

2.2 Noah model

The Noah land model is original developed in the 1980s by Oregon State University (OSU) and significant improve in recently (Ek et al., 2003b). In particular, the Cold season physics has been dramatically improved, including frozen soil and snowpack physics. Snow schemes in this version are based on the energy and mass balance of snowpack with snow compaction and sub-grid variability components. The model explicitly solves liquid water retention and percolation with the snowpack. Snow albedo

is computed based on the snow-covered fraction. The shading of vegetation is also taken account into the albedo. The upper limit of snow albedo is set to a maximum 0.44 at snow conditions. However, snow interception, drip and melt on canopy are neglected in the Noah model(Koren et al., 1999). This version of Noah model was evaluated in the GSWP-2, and its simulation skill of soil moisture was found among the best of the models ((Dirmeyer et al., 2006)

2.3 CLM model

CLM (Oleson et al. 2008) is the so called " third generation" land surface model which explicit represent the role of carbon and nitrogen in the model compared with "second generation" model, such as SSiB and Noah which are built only explicit description of soil and vegetation process involved in the closure of the surface energy and water budgets. The model has 10 soil layers and 5 snow layers depending on snow depth. CLM 3.5 applies a two-stream approximation for radiative transfer calculation. Snow albedo is based on the diffuse, direct band separate and snow age (Oleson et al., 2004). The vegetation effect is account for in snow accumulation, melt and interception through fall and drip by canopy. CLM calculates the water transfer between snow layers, infiltration, runoff, and sub-surface drainage although the water vapor transport within the snowpack is neglected.

2.4 Signal-to-Noise Ratio of multi-model results

The usefulness of the GLDAS data set has been demonstrated in weather and sub-seasonal forecasts (de Goncalves et al., 2006; Koster et al., 2004). Previous evaluations by Berg et al. (2005) suggested that soil moisture estimates using Mosaic with bias-corrected hydro-meteorological forcing data are in good agreement with in situ measurements at 1-m depth, and in general statistical agreement with satellite observations of surface soil moisture. However, the quality and accuracy of GLDAS over the TP has not been validated even before due to lack of field observations in this tough region where there are almost no available systematic observations in land surface states and fluxes.

As the main bridge of land-atmosphere interaction, the sensible and latent heat fluxes play very important roles at land surface processes. Interannual variation of these fluxes is an important issue in the study of climate dynamics. However, lack of observation makes it difficult to quantitative studies this issue over the TP. Field observations of fluxes at northern Tibet during GAME/Tibet (GEWEX Asian Monsoon Experiment on the Tibetan Plateau) and the CAMP/Tibet (CEOP Asia-Australia Monsoon Project (CAMP) on the Tibetan Plateau) (Ma and Ma, 2006; Ma et al., 2005) can only provide limited information for annual variability.

Inspired by ensemble forecast or super ensemble forecast (ensemble forecast based on different models), We try to analyze GLDAS data as “Super data assimilation” to evaluate the model skills and deficiencies over the TP where there are almost no traditional data available for validation.

Let the analysis matrix be X_{nk}, where k is the number of verification times(here are 30 years) and n is the different model (here are 3 models, CLM, Noah and Mosaic). Then the analysis mean is

$$\tilde{\mu}_f(k) = \frac{1}{N}\sum_{n=1}^{N} X_{nk}$$

the Grand or Climatological mean is

$$\tilde{\mu}_c = \frac{1}{NK}\sum_{k=1}^{K}\sum_{n=1}^{N} X_{nk}$$

The difference between the ensemble mean and climatological mean is the estimated signal. The estimated signal variance is

$$\left\langle (\tilde{\mu}_f - \tilde{\mu}_c)^2 \right\rangle = \frac{1}{K}\sum_{k} (\tilde{\mu}_f(k) - \tilde{\mu}_c)^2$$

The difference between an individual member and its corresponding ensemble mean is called the noise. The estimated noise variance is

$$\left\langle (\hat{\sigma}_f{}^2) \right\rangle = \frac{1}{NK}\sum_{n}\sum_{k} (X_{kn} - \tilde{\mu}_f(k))^2$$

this implies that the estimated signal-to noise ratio is

$$SNR = \frac{N\sum_{k} (\tilde{\mu}_f(k) - \tilde{\mu}_c)^2}{\sum_{n}\sum_{k} (X_{nk} - \tilde{\mu}_f(k))^2}$$

the f-statistic under the null hypothesis of no predictability (utilities) has distribution(DelSole and Tippett, 2008)

$$SNR\frac{K(N-1)}{K-1} \sim F_{K-1,K(N-1)}$$

the critical values reject the null hypothesis for 5% and 1% significance are list as below:

N: number of ensemble members = 3 K: number of years = 30

Confidence interval (Pval)	F-statistic	Signal-to-Noise Ratio (SNR)	Signal-to-Total Ratio (STR)
5%	1.75	0.84	0.46
1%	2.23	1.07	0.51

Figure 1 shows the Signal-to-Noise Ratio (SNR) for latent heating and sensible heating reanalysis over Tibetan Plateau during spring (MAM). The dash line indicates 3000m elevation. The SNR is estimated by CLM, Noah, and Mosaic model during 1979-2008. In the most area of the TP, the SNR for LE are larger than 1% significance in null hypothesis testing. In particular, there are significant signals in the internal part of the TP and northern part of TP. Only few regions in the south-east part of TP have no significant signal. Similar to the LE, the SNR of SH are larger than 1% significance except some regions in the west and south part of the TP. The SNR analysis implies the signals from interannual change are large than noise within the different models. As a result, the GLDAS reanalysis could be used to analyze the interannual variability over the TP.

3. Annual variability of water and energy budget over the TP

In this study, we define the area of the TP as the region with an elevation higher than 3000m. This overall area occurs in a domain between 70-110°E longitude and 25-45°N latitude. Major mountains in this region include the Himalayas in the southern edge of the TP, and the Karakoram and Kunlun mountains in the western and northern edges. The Pamir, Karakoram, Kunlun and Tianshan ridges are adjacent in the west part of the TP. The Qilian Mountain separates the Gobi desert from the TP in the northeastern edge. Two large subregions, the Qaidam basin and Yarlung Zangbo Valley, are located in the north-eastern and southeastern part of the TP, respectively.

3.1 water balance

The land surface water balance is expressed as

$$W = P - E - R$$

$$R = QS + QSB$$

where W denotes surface water storage, which includes soil moisture, snow water equivalent and canopy water; P is precipitation; E represents evapotranspiration from bare soil, lakes and vegetation as well as surface snowpack sublimation; R is runoff including the surface (QS) and subsurface flow (QSB).

Figure 2 shows the annual cycle of evapotranspiration, surface runoff, subsurface runoff, and surface water storage over the TP based on three models during 1979-2008.

Precipitation forcing (rainfall rate and snowfall rate) is not shown since it's same for all three models.

The monthly mean evapotranspiration shows a prominent seasonal cycle with precipitation change. In the winter months (December–February), the Evapotranspiration is less than 0.5 mm/day. During the summer (June–August) maxima, it reaches over 1.5 mm/day exhibiting a significant magnitude change in annual cycle. The three models show some differences in the estimation of evapotranspiration. The Mosaic model tends to overestimate and Noah model tends to underestimate.

In the estimation of surface runoff, the three models show a pretty large departure with each other. The Noah model tends to overestimate the surface runoff with a maximum 0.7mm/day during June-July. On the other hand, the Mosaic model underestimates the runoff only to 0.2 mm/day at maximum.

The Subsurface runoff (QSB) also shows a similar large difference with the surface runoff. However, the maximum of subsurface runoff shows a rough 2 months delay comparing with the surface runoff. The huge difference in both surface and subsurface runoffs demonstrates the large model bias in the runoff parameterization in this region. Due to lack of the in-situ observation of river discharge, we cannot judge which model is more realistic. Based on the analysis of Feng and Houser (2008), CLM model demonstrates more accurately over the Mississippi river basin during GSWP-2 project.

Surprisingly, the three models show consistent analysis of surface water storage with a remarkable two-peak feature of the seasonal surface water storage. The surface water stores as snow pack in winter with a maximum and depletes in spring, and then the

surface is recharged with convection rainfall in the summer and discharged by subsurface runoff in the autumn.

Although the models show pretty big differences at runoff, the simulated ET and surface water storage as the main components for land-climate interaction are good agreed and balanced over the annual cycle.

3.2 Energy balance

The surface energy equation is written as

$$R = SWnet + LWnet - SH - LE - G - U$$

Where R represents the energy balance residual; SWnet and LWnet are the net shortwave and longwave radiation, respectively; LE represents the surface latent heat flux, SH the sensible heat flux, G the ground heat flux, and U the miscellaneous term such as snow phase change heat flux. The magnitudes of the annual averages of R is close to zero, thus only the net radiations, heat fluxes, and miscellaneous term are shown in Figure 3.

All models are similar in capturing the strong seasonal cycle in each energy budget component. The net shortwave radiation, SWnet, gains a peak in May-June over the TP instead of in summer over the most regions in northern hemisphere. All models show almost same cycle in the net shortwave radiation. This implies the treatment of surface albedo is quite agreed in each model while the large discrepancy is noted in CLM model. This difference in CLM models indicates the model's uncertainty in snow albedo parameterization when it presents snow.

The simulated net longwave radiation varies considerably in three models. Mosaic model produces less negative net longwave radiation indicating a colder surface; CLM has the largest negative net longwave radiation in the summer as a result of the warmer surface. Positive bias in net shortwave radiation in CLM is partially compensated by the negative bias at the longwave radiation.

The seasonal cycle of sensible and latent heat fluxes appear to follow the seasonal variation of the surface net radiation (SWnet+LWnet). However, the maximum sensible heating appears in May, whereas the maximum latent heating locates in July. The strong latent heat flux in Mosaic is consistent with its largest evaporation (Figure 2). All models show the same transience of ground heat flux from negative to positive, and vice versa during summer to winter.

Although the magnitude of miscellaneous term is small, Noah model show pretty significant differences with other two models. In the CLM and MOS, the heat flux of snow phase change is very small (rough 10^-2 W/m^2) indicating that most of the snow is removed by sublimation. However, the Noah model simulates a realistic snow-melting peak at April.

3.3 Summary

Based on the analysis above, the characteristic of the annual cycle of energy balance over the TP could be summarized as: located at mid-latitude (29-43N), the Tibetan Plateau receive a strong annual cycle in net shortwave radiation comparing to the relative flat change in net long wave radiation. The sensible heating is much larger than latent heating over the Tibetan Plateau. The sensible heating has a peak at May,

distinguishing with the latent heating maximum at July-August. From February to August, the grand flux is positive which means the net energy budget is warm up the soil; whereas the heat is take out from soil during September to January. These characteristics are well agreed with the field observations of fluxes at northern Tibet during GAME/Tibet GEWEX Asian Monsoon Experiment on the Tibetan Plateau) and the CAMP/Tibet (CEOP Asia-Australia Monsoon Project (CAMP) on the Tibetan Plateau) (Ma and Ma, 2006; Ma et al., 2005).

The latitude-time sections of the sensible and latent fluxes are also analyzed (figure not show). From winter to summer, the sensible flux is intensified from the south and gradually moves to the north part of the TP. There are two distinguished maximums of sensible heating: The first one exists near 30°N in May although the intensity is relatively weak; the second one locates near 40°N during July-August with a magnitude more than 100 w/m^2. On the other hand, there is only one peak of the latent heat flux during summer. The maximum of latent flux located at the south part of the TP, whereas there is no significant latent flux at the north part of the TP.

The annual cycle of water balance over the TP could be summarized as: the rainfall rate from atmospheric forcing shows a peak in July with rough 2.5 mm/day and a minimum close to zero during wintertime. In contract, the snowfall rate shows a large value during winter and a minimum in the summer. The peak of snowfall is in March that agrees with observations: more frequently serious snowstorm happens at early spring since the warm moist air from the southern region frequently invades to the north during season transience. Due to high elevation, there are still some snowfalls during summer

over the TP (rough 0.1mm/day). Correspondingly, the evapotranspiration and runoff also show similar pattern with rainfall rate during the annual cycle. In the whole year, the water loss due to evapotranspiration is much larger than runoff. Since the sublimation of snowpack, there is still significant evaporation over the TP during the wintertime.

4 Heat source/sink transition

In the decades before, Chinese distinguished scientist Ye Duzhen firstly found that the land surface processes over the Tibetan Plateau act as a strong "elevated" heat source to the atmosphere in summer based on the analysis from limited meteorological data available over Tibet. This conclusion confirmed by the analysis of Asian monsoon processes by Flohn (1957). Ye and Gao (1979) further inferred the land surface over Tibetan Plateau acts as a heat sink in winter due to snow albedo effect similar to the Polar Regions. This famous hypothesis plays an important role to explain the mechanism of winter Asian monsoon circulation, but it has never been observed in-situ.

From the GLDAS three model's reanalysis, either monthly mean total heat flux to atmosphere (SH+LW) or sensible heat flux over the TP is positive during all season. However, there are 11 grid points in the west edge of the TP where the monthly mean sensible heat fluxes are negative in January. Similarly, there are 4 grid points where the monthly mean latent heat flux is negative. The monthly mean total fluxes (sensible plus latent heat) are negative at 7 grid points during January (figure 4). These grid points are mainly located at the joint region of Himalaya and Karakoram Mountain in the west edge of the TP where exists the largest glaciered region outside of the Polar Regions.

General speaking, the land surface experienced the shift between heat source/sink daily with the diurnal change of incident solar radiations. When sun illustrates on the land surface, the net radiation is positive that requires the sensible heat and latent heat to convey the extra energy to the atmosphere. During the night, however, the net radiation on the land surface is negative which must be compensated by the heat fluxes from atmosphere. Whereas in the monthly scale, in the same latitude regions (25-45°N) the monthly mean sensible flux and latent flux are positive even during winter. Due to the atmospheric column is pure radiative cooling (net radiative loss) at troposphere, without surface heat flux or deficient surface heat flux will make the whole atmosphere is net heat loss. This net heat loss relative to its surrounding will result horizontal temperature gradients and induce a vertical circulation that converge heat aloft and maintain thermal equilibrium through sinking motion and adiabatic compression On the other hand, the net heat gain due to large surface heating will introduce the ascend motion in vertical. The shift between heat sink and source are basic for the hypothesis of the plateau monsoon, the seasonal shift of the vertical motion around the TP (Tang and Reiter, 1984).

5 Budyko diagram

The characters of annual water balance are represented on the so-called Budyko diagram that presents the ratio of evaporation/precipitation (E/P) as a function of the ratio of potential evaporation/precipitation (Ep/P). Budyko (1974) assumed that actual evaporation is controlled by both water and energy availabilities. At the annual time

330 scale, the water availability is the amount of annual precipitation and the energy
331 availability can be measured by the potential evaporation.

332 Ratio E/P measures the way that rainfall is partitioned into evaporation and runoff.
333 On the other hand, the ratio Ep/P is a measure of climate, also called the dryness index
334 (or index of dryness). Large Ep/P (>1) represents dry or arid climate, while small Ep/P
335 (<1) represents a wet or humid climate. Thus the Budyko diagram encapsulates a major
336 climatic control on annual water balance.

337 Figure 5 showes the Budyko diagram over the TP. The green plus signs represent
338 each grid point at the TP. The red dash line is Budyko curve. The dryness index in most
339 of part of the TP are greater than 1 except a few points in the southern edge. This
340 indicates the TP has a typical dry or arid climate where the evaporation is mainly
341 controlled by the precipitation. The only few grid points with dryness index less than 1
342 are located in the south-east edge of The TP where the moist air from the south climbs
343 along the Yalung Zangbo village producing relatively large amount of precipitation.

344

345 6. Conclusions

346 Based on newly produced reanalysis land surface states and fluxes by Global
347 Land Data Assimilation System, the energy and water budget over the TP are quantitative
348 studied in this paper. Three different models, CLM, Mosaic and Noah model's reanalysis
349 data are compared over this special region TP, the largest and highest plateau around the
350 world.

All three models well catch the annual cycle over the TP both in the water and energy budget. However, it still shows pretty large difference in the hydrological component, including the surface and subsurface runoff. In the most of the TP, Signal-Noise-Ratios estimated by three models during 1979-2008 are larger than 1% significance in null hypothesis testing. In particular, there are significant signals in the internal part of the TP and northern part of TP. The GLDAS reanalysis data could be used to analyze the interannual variability over the TP.

Located at mid-latitude (29-43N), the Tibetan Plateau receive a strong annual cycle in net shortwave radiation comparing to the relative flat change in net long wave radiation. The sensible heating is much larger than latent heating over the Tibetan Plateau. The sensible heating has two peaks: one is at May near 30N and another is during summer in the north part of the TP. It is distinguishing with the only maximum of latent heating at July-August. From February to August, the ground flux is positive which means the net energy budget is warm up the soil; whereas the heat is take out from soil during September to January.

There are some grid points that the monthly mean of total fluxes (sensible plus latent) are negative during winter. These grid points are mainly located at the joint region of Himalaya and Karakoram Mountain in the west edge of the TP where exists the largest glaciered region outside of the Polar Regions. The GLDAS provide another prove for the famous hypothesis: the TP acts as a heat sink during winter. This special character of the land thermal forcing would induce the large-scale descending motion as suggested by plateau monsoon.

At the annual hydrological cycle, the rainfall from atmospheric shows a single peak in July and the minimum close to zero during wintertime. In contract, the snowfall shows a large value during winter and a minimum in the summer. Due to the high elevation, there are still some snowfalls during summer over the TP. In the whole year, the water loss due to evapotranspiration is much larger than runoff. Since the sublimation of snowpack, there is still significant evaporation over the TP during the wintertime.

The TP is a typical dry or arid climate where the evaporation is mainly controlled by the precipitation. Based on the budyko diagram, the only few grid points with dryness index less than 1 are located in the south-east edge of the TP where the moist air from the south climbs along the Yalung Zangbo village producing relatively large amount of precipitation. Over the most of TP, the Bowen ratios are far larger than 1.

Acknowledgments

Authors would like to thank Paul Houser and Randy Koster for their insightful discussion about GLDAS data. The GLDAS data used in this study were obtained from NASA's Earth Science Division and archived and distributed by the Goddard Earth Sciences (GES) Data and Information Services Center (DISC). This study is partially supported by China National Public Benefit Research Foundation (No.GYHY200906018) and an open project of the Institute of Plateau Meteorology.

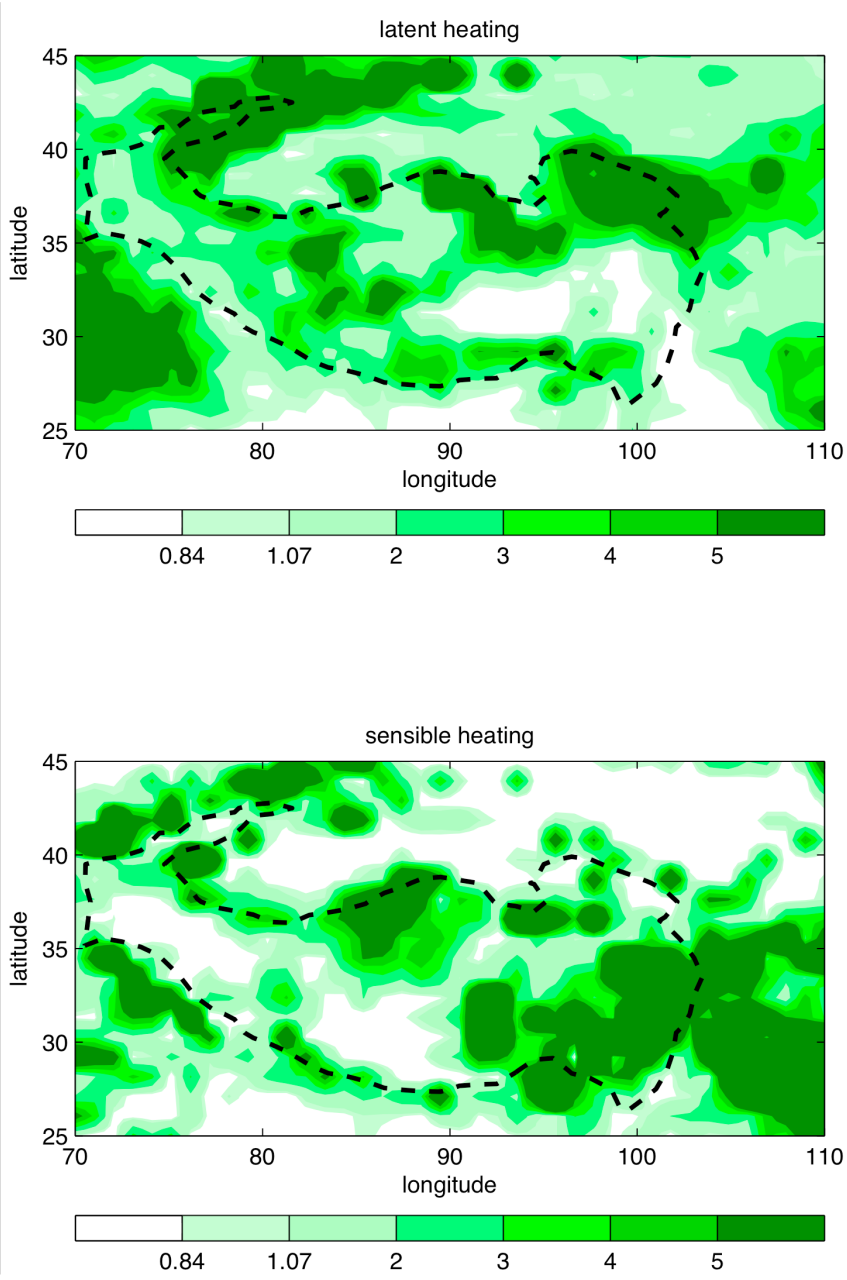

Figure 1. Signal-to-Noise Ratio (SNR) for GLDAS latent heating and sensible heating over the Tibetan Plateau during spring (MAM). The dash line indicates 3000m elevation. The SNR is estimated by CLM, Noah and Mosaic model during 1979-2008.

399 The f-statistics testing for null hypothesis is 0.84 and 1.07 for 95% and 99%

400 significance.

401

402

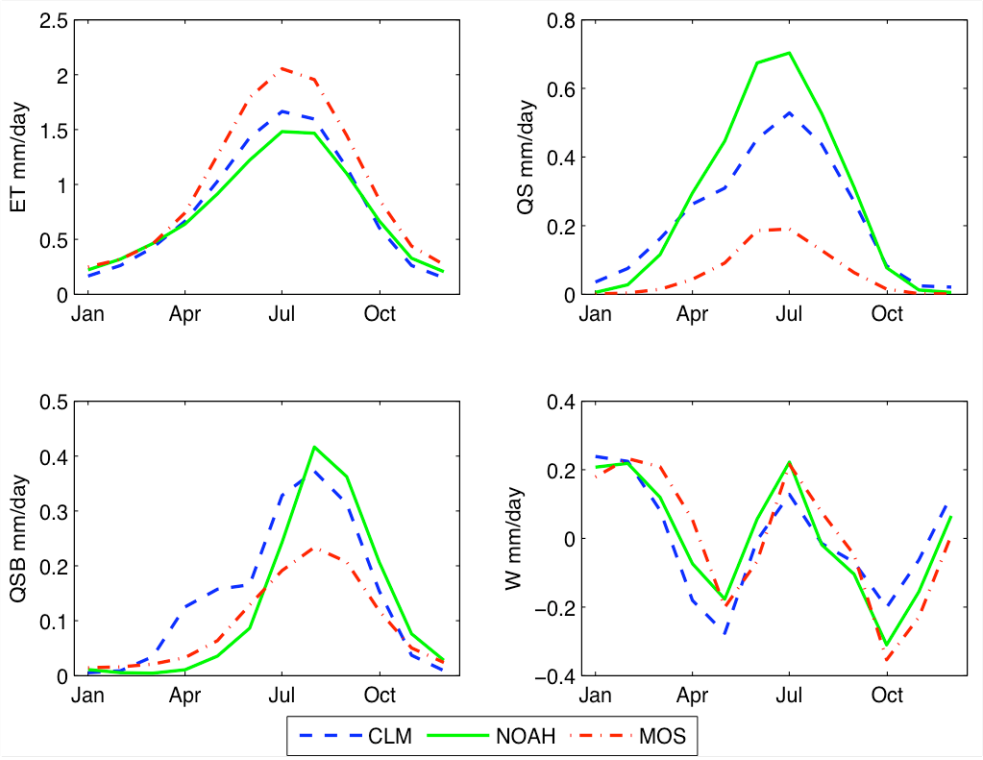

403

404

405 Figure 2. The annual cycle of each component of water budget over the Tibetan

406 Plateau: total evapotranspiration (ET, upper-left), surface runoff (QS, upper-right)

407 ,subsurface runoff (QSB, bottom-left) and water storage at land surface (W, bottom-

408 right).

409

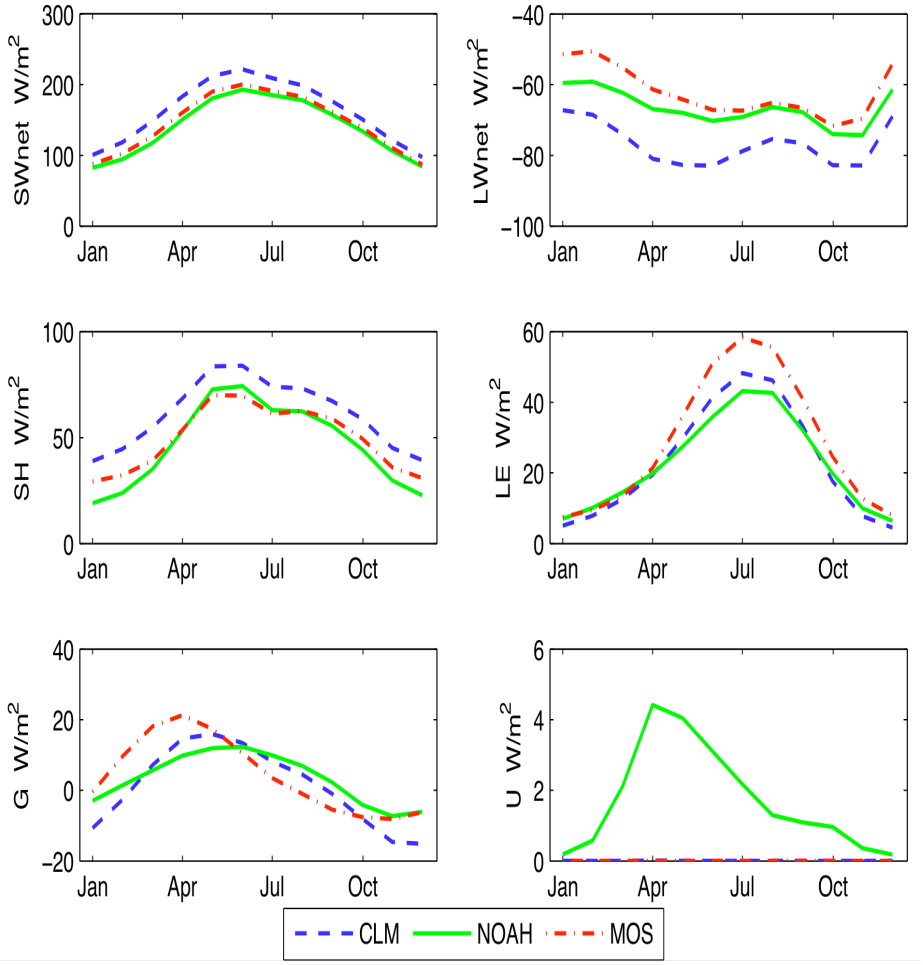

Figure 3. The annual cycle of each component of energy budget over the Tibetan Plateau: net shortwave radiation (SWnet, upper-left), net longwave radiation (LWnet, upper-right), Sensible heat flux (SH, center-left), Latent heat flux (LE, center-right), Ground heat flux(G, bottom-left) and miscellaneous term such as snow phase change caused heat flux (U, bottom-right).

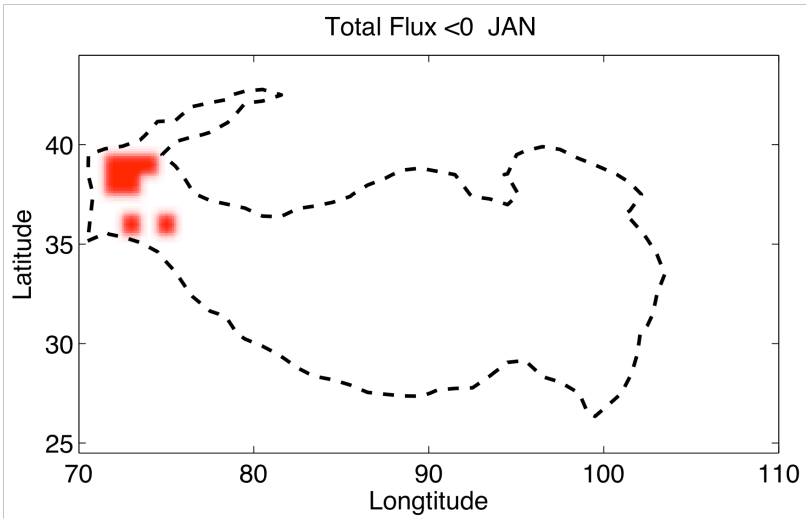

Figure 4. Monthly mean total heat flux (sensible +latent) is negative in January (total 7 grid points). These grid points locate at the joint region of Himalaya and Karakoram maintain in the west edge of the TP where exist the largest glaciered region outside of the Polar Regions. There are also 5 grid points are negative at December and February respectively.

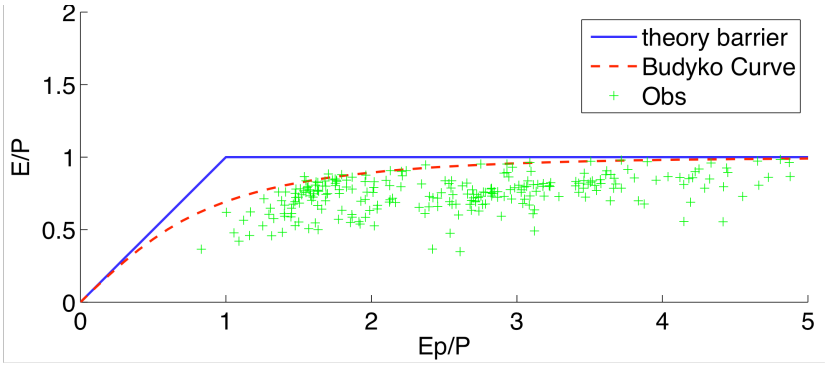

Figure 5. Bukyko diagram over the Tibetan Plateau. The green plus signs represent the each grid point at the TP. The red dash line is Budyko curve.

433

434 Reference

435 Berg, A.A., Famiglietti, J.S., Rodell, M., Reichle, R.H., Jambor, U., Holl, S.L. and Houser,
436 P.R., 2005. Development of a hydrometeorological forcing data set for global
437 soil moisture estimation. International Journal of Climatology, 25(13): 1697-
438 1714.
439 Chen, F., Mitchell, K., Schaake, J., Xue, Y., Pan, H.L., Koren, V., Duan, Q.Y., Ek, M. and
440 Betts, A., 1996. Modeling of land surface evaporation by four schemes and
441 comparison with FIFE observations. Journal of Geophysical Research. D.
442 Atmospheres, 101: 7251-7268.
443 Dai, Y., Zeng, X., Dickinson, R.E., Baker, I., Bonan, G.B., Bosilovich, M.G., Denning, A.S.,
444 Dirmeyer, P.A., Houser, P.R., Niu, G., Oleson, K.W., Schlosser, C.A. and Yang, Z.-
445 L., 2003. The Common Land Model. Bulletin of the American Meteorological
446 Society, 84(8): 1013-1023 %U http://dx.doi.org/10.1175%2FBAMS-84-8-
447 1013.
448 de Goncalves, L.G.G., Shuttleworth, W.J., Chou, S.C., Xue, Y.K., Houser, P.R., Toll, D.L.,
449 Marengo, J. and Rodell, M., 2006. Impact of different initial soil moisture
450 fields on Eta model weather forecasts for South America. Journal of
451 Geophysical Research-Atmospheres, 111(D17): 14.
452 DelSole, T. and Tippett, M.K., 2008. Predictable Components and Singular Vectors.
453 Journal of the Atmospheric Sciences, 65(5): 1666-1678 %U
454 http://dx.doi.org/10.1175%2F2007JAS2401.1.
455 Dirmeyer, P.A., Gao, X., Zhao, M., Guo, Z., Oki, T. and Hanasaki, N., 2006. GSWP-2:
456 Multimodel Analysis and Implications for Our Perception of the Land Surface.
457 Bulletin of the American Meteorological Society, 87(10): 1381-1397 %U
458 http://dx.doi.org/10.1175%2FBAMS-87-10-1381.
459 Ek, M.B., Mitchell, K.E., Lin, Y., Grunmann, P., Rogers, E., Gayno, G., Koren, V. and
460 Tarpley, J.D., 2003a. Implementation of the upgraded Noah land-surface
461 model in the NCEP operational mesoscale Eta model. J. Geophys. Res, 108:
462 8851.
463 Ek, M.B., Mitchell, K.E., Lin, Y., Rogers, E., Grunmann, P., Koren, V., Gayno, G. and
464 Tarpley, J.D., 2003b. Implementation of Noah land surface model advances in
465 the National Centers for Environmental Prediction operational mesoscale Eta
466 model. Journal of Geophysical Research-Atmospheres, 108(D22): 16.
467 Feng, X. and Houser, P., 2008. An investigation of GSWP-2 Mississippi River basin
468 surface water and energy budgets. Journal of Geophysical Research-
469 Atmospheres, 113(D15): -.
470 Flohn, H., 1957. Large-scale aspects of the “summer monsoon” in South and East
471 Asia. J. Meteor. Soc. Japan, 35: 180–186.
472 Hahn, D.G. and Shukla, J., 1976. An Apparent Relationship between Eurasian Snow
473 Cover and Indian Monsoon Rainfall. Journal of the Atmospheric Sciences,
474 33(12): 2461-2462.

475 Koren, V., Schaake, J., Mitchell, K., Duan, Q.Y., Chen, F. and Baker, J.M., 1999. A
476 parameterization of snowpack and frozen ground intended for NCEP weather
477 and climate models. Journal of Geophysical Research-Atmospheres,
478 104(D16): 19569-19585.
479 Koster, R.D. and Suarez, M.J., 1996. The Influence of Land Surface Moisture
480 Retention on Precipitation Statistics. Journal of Climate, 9(10): 2551-2567
481 %U http://dx.doi.org/10.1175%2F1520-
482 0442%281996%29009%3C2551%3ATIOLSM%3E2.0.CO%3B2.
483 Koster, R.D., Suarez, M.J., Liu, P., Jambor, U., Berg, A., Kistler, M., Reichle, R., Rodell, M.
484 and Famiglietti, J., 2004. Realistic Initialization of Land Surface States:
485 Impacts on Subseasonal Forecast Skill. Journal of Hydrometeorology, 5(6):
486 1049-1063.
487 Ma, W.Q. and Ma, Y.M., 2006. The annual variations on land surface energy in the
488 northern Tibetan Plateau. Environmental Geology, 50(5): 645-650.
489 Ma, Y., Fan, S., Ishikawa, H., Tsukamoto, O., Yao, T., Koike, T., Zuo, H., Hu, Z. and Su, Z.,
490 2005. Diurnal and inter-monthly variation of land surface heat fluxes over
491 the central Tibetan Plateau area. Springer Wien, pp. 259-273.
492 Oleson, K., Dai, Y., Bonan, G., Bosilovich, M., Dickinson, R., Dirmeyer, P., Hoffman, F.,
493 Houser, P., Levis, S. and Niu, G.Y., 2004. Technical Description of the
494 Community Land Model (CLM). Technical Note NCAR/TN-461+ STR. National
495 Center for Atmospheric Research.
496 Rodell, M., Houser, P.R., Jambor, U., Gottschalck, J., Mitchell, K., Meng, C.J., Arsenault,
497 K., Cosgrove, B., Radakovich, J. and Bosilovich, M., 2004. The Global Land Data
498 Assimilation System. Bulletin of the American Meteorological Society, 85(3):
499 381-394.
500 Sellers, P.J., Los, S.O., Tucker, C.J., Justice, C.O., Dazlich, D.A., Collatz, G.J. and Randall,
501 D.A., 1996. A Revised Land Surface Parameterization (SiB2) for Atmospheric
502 GCMS. Part II: The Generation of Global Fields of Terrestrial Biophysical
503 Parameters from Satellite Data. Journal of Climate, 9(4): 706-737 %U
504 http://dx.doi.org/10.1175%2F1520-
505 0442%281996%29009%3C0706%3AARLSPF%3E2.0.CO%3B2.
506 Tang, M. and Reiter, E.R., 1984. Plateau Monsoons of the Northern Hemisphere: A
507 Comparison between North America and Tibet. Monthly Weather Review,
508 112(4): 617-637 %U http://dx.doi.org/10.1175%2F1520-
509 0493%281984%29112%3C0617%3APMOTNH%3E2.0.CO%3B2.
510 Wu, T.-W. and Qian, Z.-A., 2003. The Relation between the Tibetan Winter Snow and
511 the Asian Summer Monsoon and Rainfall: An Observational Investigation.
512 Journal of Climate, 16(12): 2038-2051 %U
513 http://dx.doi.org/10.1175%2F1520-
514 0442%282003%29016%3C2038%3ATRBTTW%3E2.0.CO%3B2.
515 Xie, L., Yan, T., Pietrafesa, L.J., Karl, T. and Xu, X., 2005. Relationship between
516 western North Pacific typhoon activity and Tibetan Plateau winter and
517 spring snow cover. Geophys. Res. Lett., 32(16): 1-4.
518 Xu, X., Zhang, R., Koike, T., Lu, C., Shi, X., Zhang, S., Bian, L., Cheng, X., Li, P. and Ding,
519 G., 2008. A New Integrated Observational System Over the Tibetan Plateau.

Bulletin of the American Meteorological Society, 89(10): 1492-1496 %U http://dx.doi.org/10.1175%2F2008BAMS2557.1.

Yasunari, T., 2007. Role of land-atmosphere interaction on Asian monsoon climate. Journal of the Meteorological Society of Japan, 85B: 55-75.

Ye, D. and Gao, Y., 1979. The Meteorology of the Qinghai-Xizang (Tibet) Plateau. Science Press, Beijing.